8790 *Inorg. Chem.* **2010**, *49*, 8790–8801
DOI: 10.1021/ic100944d

Inorganic Chemistry
Article

Dinuclear Copper(I) Complexes Containing Cyclodiphosphazane Derivatives and Pyridyl Ligands: Synthesis, Structural Studies, and Antiproliferative Activity toward Human Cervical and Breast Cancer Cells

Maravanji S. Balakrishna,*,† D. Suresh,† Ankit Rai,‡ Joel T. Mague,§ and Dulal Panda*,‡

†*Phosphorus Laboratory, Department of Chemistry,* ‡*Department of Biosciences and Bioengineering, Indian Institute of Technology Bombay, Mumbai 400 076, India, and* §*Chemistry Department, Tulane University, New Orleans, Louisiana 70118*

Received May 12, 2010

Several mixed-ligand copper(I) complexes of cyclodiphosphazanes, $[^{t}BuNP(NC_4H_8X)]_2$ (**1**, X = O; **2**, X = NMe), were synthesized by reacting the octanuclear copper(I) complexes $[Cu_8(\mu_2\text{-}I)_8\{[^{t}BuNP(NC_4H_8X)]_2\}_4]$ (**3**, X = O; **4**, X = NMe) with various pyridyl ligands. Interaction of the metallomacrocyclic complex **3** or **4** with pyridine, 2,2′-bipyridine, and 1,10-phenanthroline afforded the neutral dinuclear complexes $[(C_5H_5N)_4Cu_2I_2\{[^{t}BuNP(NC_4H_8X)]_2\}]$ (**5**, X = O; **6**, X = NMe), $[(2,2'\text{-bpy})_2Cu_2I_2\{[^{t}BuNP(NC_4H_8X)]_2\}]$ (**7**, X = O; **8**, X = NMe), and $[(1,10\text{-phen})_2Cu_2I_2\{[^{t}BuNP(NC_4H_8X)]_2\}]$ (**9**, X = O; **10**, X = NMe), respectively, in good yield. The new dinuclear complexes **3**, **5**, and **7**−**9** were tested for their cytotoxic properties against human cervical cancer (HeLa) cells. The results indicated that all of the copper complexes have in vitro antitumor activity either similar to or better than that of cisplatin, a widely used anticancer drug. Among the compounds tested, complex **9** showed the most potent inhibitory activity in HeLa cells. In addition, complex **9** was found to potently inhibit proliferation of human breast cancer cells (MCF-7), highly metastatic breast cancer cells (MDA-MB 231), and nontransformed Chinese hamster ovary (CHO) cells. Complex **9** inhibited proliferation of these cells in culture more potently than cisplatin; for example, complex **9** was found to inhibit proliferation of HeLa and MCF-7 cells 3 and 5 times more efficiently than cisplatin. Complex **9** treatment damaged the DNA integrity, blocked the cells in the G1 phase of the cell cycle, and induced apoptosis via a p53-dependent pathway. The molecular structures of complexes **9** and **10** were confirmed by single-crystal X-ray diffraction studies.

Introduction

The role of transition-metal complexes in diagnosis, medicine, and chemotherapy is well documented.[1−4] Cisplatin, carboplatin, and other platinum-based antitumor drugs are highly active toward testicular cancers[5−7] and are also effective against a wide range of other tumors such as ovarian, bladder carcinoma, and non-small-cell lung cancer.[8] However, treatment failure is often caused by the development of resistance to these complexes[9] and is also due to their high nephrotoxicity and neurotoxicity.[5,10] As a result, it is necessary to design metallodrugs that are less toxic and highly active in smaller dosage, especially against cell lines that have acquired high resistance to cisplatin. In this context, attention has been drawn toward group 11 metals[4,11] for cancer therapy owing to the long known utility of gold complexes in the treatment of tuberculosis, arthritis, and, in the 1970s, P388 leukemia.[12] Later, Sadler and others have extensively studied the antitumor activity of several gold(I) complexes containing phosphine ligands.[4,10,13]

Copper complexes are potential reagents for the cleavage of DNA both oxidatively[14,15] and hydrolytically.[16−18] Many of these complexes are found to be anti-inflammatory,[19]

*To whom correspondence should be addressed. E-mail: krishna@chem.iitb.ac.in or msb_krishna@iitb.ac.in (M.S.B.), panda@iitb.ac.in (D.P.). Fax: +91-22-5172-3480/2576-7152 (M.S.B.), +91-22-5172-3480 (D.P.).

(1) Clarke, M. J.; Zhu, F.; Frasca, D. R. *Chem. Rev.* **1999**, *99*, 2511–2533.
(2) Mascini, M.; Bagni, G.; Pietro, M. L. D.; Ravera, M.; Baracco, S.; Osella, D. *Biometals* **2006**, *19*, 409–418.
(3) Farver, O. *Textbook of Drug Design and Discovery*, 3rd ed.; Taylor & Francis Ltd.: London, U.K., 2002; pp 364−409.
(4) Guo, Z.; Sadler, P. J. *Advances in Inorganic Chemistry*; Academic Press: San Diego, CA, 2000; Vol. *49*, pp 183−306.
(5) Lippert, B. *Cisplatin: Chemistry and biochemistry of a leading anticancer drug*; Wiley-VCH: Weinheim, Germany, 1999.
(6) Matsumoto, K.; Sakai, K. *Advances in Inorganic Chemistry*; Academic Press: San Diego, CA, 2000; Vol. *49*, pp 375−427.
(7) Ho, J. W. *Recent Pat. Anti-Cancer Drug Discovery* **2006**, *1*, 129–134.
(8) Ardizzoni, A.; Antonelli, G.; Grossi, F.; Tixi, L.; Cafferata, M.; Rosso, R. *Ann. Oncol.* **1991**, *10*, S13–S17.
(9) Kelland, L. R. *Crit. Rev. Oncol. Hematol.* **1993**, *15*, 191–219.
(10) Sadler, P. J.; Guo, Z. *Pure Appl. Chem.* **1998**, *70*, 863–871.
(11) Brewer, G. J. *Exp. Biol. Med.* **2001**, *226*, 665–673.
(12) Simon, T. M.; Kunishima, D. H.; Vibert, G. J.; Lober, A. *Cancer Res.* **1981**, *41*, 94–97.
(13) Berners-Price, S. J.; Mirabelli, C. K.; Johnson, R. K.; Mattern, M. R.; McCabe, F. L.; Faucette, L. F.; Sung, C. M.; Sadler, P. J.; Crooke, S. T. *Cancer Res.* **1986**, *46*, 5486–5489.

 Published on Web 09/02/2010

antiarthritic, antiulcer,[20] anticonvulsant, and antitumor agents.[21] The selective permeability of cancer cell membranes to copper complexes[22] and their strict regulations of the intracellular concentration have encouraged the synthesis of copper-based drugs as potential anticancer agents that are anticipated to have less severe side effects than standard anticancer drugs. Several copper(I) complexes containing either pyridyl-type ligands such as 1,10-phenanthraline[23] or mono- and bis(phosphine) ligands were screened for their anticancer activity,[13−26] and some have shown good antiproliferative activity toward cancer cells.

Because of the nonavailability of mechanistic details on the antitumor activity of copper complexes, it is premature to talk about the choice of ligands employed in these studies. It is important to note that copper has not been shown to cause cancer in human beings or in animals and the international agency for research on cancer has not classified copper as a human carcinogen. Therefore, it is appropriate to design anticancer drugs based on copper because these are anticipated to cause lower toxic effects. Further, ligands designed with carefully chosen organic substituents are not expected to cause nephrotoxicity in human beings. Because copper complexes containing either phosphines[26−29] or pyridyl-type ligands showed moderate anticancer activities, we considered that the mixed-ligand complexes containing both phosphines and pyridyl-type ligands would be good candidates for examination of their effect(s) on cell proliferation. 2,2′-Bipyridine and 1,10-phenanthraline were obvious choices among pyridyl ligands as these compounds readily form chelates that are moderately stable with promising cytotoxic effects. In choosing the phosphines, we wanted to avoid compounds containing P−C bonds because alkylphosphines are highly corrosive and toxic and the aryl substituents are known for nephrotoxicity.[30] Phosphine ligands containing P−N bonds are less toxic and, in fact, the reservoir of phosphate, phosphacreatine $[P(O)\{NHC(NH)NCH_2COOH\}O_2]^{2-}$,[31] being a P−N-bond-containing molecule, prompted us to choose the P−N-bond-containing cyclodiphosphazanes $[RNPX)]_2$ as the bidentate ligands. Cyclodiphosphazanes or diazadiphosphetidines are nearly planar, saturated inorganic heterocycles containing alternating trivalent phosphorus and nitrogen atoms. Although P−N bonds are sensitive to acid- or base-promoted hydrolytic cleavage,[32] the rigid four-membered P_2N_2 rings are stable toward hydrolysis.

The main-group and transition-metal chemistry of cyclodiphosphazanes is well documented.[33] Recently, we have studied the antitumor activity of gold(I) and the selenoester-containing cyclodiphosphazanes and found them to inhibit the growth of cancer cells by inducing apoptosis.[34,35] Herein, we report the synthesis of various mixed-ligand dinuclear copper(I) complexes and their potent antitumor activities against several types of cancer cells in culture.

Results and Discussion

Synthesis of Metal Complexes. The direct reactions of cuprous halides with ligands **1** and **2** in the presence of pyridyl-type ligands resulted in the formation of several complexes that could not be characterized, and attempts to separate the complexes from the reaction mixture have been unsuccessful. The spectroscopic and analytical data for the reaction products revealed the presence of simple mononuclear pyridyl-type ligand-bound complexes along with insoluble cyclodiphosphazane-containing coordination polymers. This prompted us to carry out the reaction in two steps to make the desired mixed-ligand complexes. The reaction of cyclodiphosphazane ligand **1** or **2** with 4 equiv of cuprous iodide resulted in the formation of novel octanuclear metallamacrocycles **3** and **4** in good yield, which were recrystallized from acetonitrile to give analytically pure crystalline materials. The octanuclear copper(I) complexes $[Cu_8(\mu_2\text{-}I)_8(CH_3CN)_4\{[^t BuNP(NC_4H_8X)]_2\}_4]$ (**3**, X = O; **4**, X = NMe) were reacted with pyridyl-type ligands to form various mixed-ligand complexes. The reactions of an excess of pyridine with complex **3** or **4** in

(14) Pogozelski, W. K.; Tullius, W. K. *Chem. Rev.* **1998**, *98*, 1089–1107.
(15) Sigman, D. S.; Bruce, T. W.; Sutton, C. L. *Acc. Chem. Res.* **1993**, *26*, 98–104.
(16) Zhang, S.; Zhu, Y.; Tu, C.; Wei, H.; Yang, Z.; Lin, L.; Ding, J.; Zhang, J.; Guo, Z. *J. Inorg. Biochem.* **2004**, *98*, 2099–2106.
(17) Hegg, E. L.; Burstyn, J. N. *Coord. Chem. Rev.* **1998**, *173*, 133–165.
(18) An, Y.; Liu, S.-D.; Deng, S.-Y.; Ji, L.-N.; Mao, Z.-W. *J. Inorg. Biochem.* **2006**, *100*, 1586–1593.
(19) (a) Dillon, C. T.; Hambley, T. W.; Kennedy, B. J.; Lay, P. A.; Weder, J. E.; Zhou, Q. D. *Met. Ions Biol. Syst.* **2004**, *41*, 253–277. (b) Weder, J. E.; Dillon, C. T.; Hambley, T. W.; Kennedy, B. J.; Lay, P. A.; Biffin, J. R.; Regtop, H. L.; Davies, N. M. *Coord. Chem. Rev.* **2002**, *232*, 95–126.
(20) Sorenson, J. R. J.; Ramakrishna, K.; Rolniak, T. M. *Agents Actions* **1982**, *12*, 408–411.
(21) (a) Muller, A. R.; Vizcaya-Ruiz, A. D.; Plant, N.; Ruiz, L.; Dobrota, M. *Chem.-Biol. Interact.* **2007**, *165*, 189–199. (b) Marzano, C.; Pellei, M.; Colavito, D.; Alidori, S.; Lobbia, G. G.; Gandin, V.; Tisato, F.; Santini, C. *J. Med. Chem.* **2006**, *49*, 7317–7324. (c) Marzano, C.; Pellei, M.; Tisato, F.; Santini, C. *Anti-Cancer Agents Med. Chem.* **2009**, *9*, 185–211.
(22) Aplegot, S.; Coppey, J.; Fromentin, A.; Guille, E.; Poupon, M. F.; Roussel, A. *Anticancer Res.* **1986**, *6*, 159–165.
(23) Devereux, M.; Shea, D. O.; Kellett, A.; McCann, M.; Walsh, M.; Egan, D.; Deegan, C.; Kedziora, K.; Rosair, G.; Muller-Bunz, H. *J. Inorg. Biochem.* **2007**, *101*, 881–892.
(24) Sanghamitra, N. J.; Phatak, P.; Das, S.; Samuelson, A. G.; Somasundaram, K. *J. Med. Chem.* **2005**, *48*, 977–985.
(25) Snyder, R. M.; Mirabelli, C. K.; Johnson, R. K.; Sung, C. M.; Faucette, L. F.; McCabe, F. L.; Zimmerman, J. P.; Whiteman, M.; Hempel, J. C.; Crooke, S. T. *Cancer Res.* **1986**, *46*, 5054–5060.
(26) Adwankar, M. K.; Wycliff, C.; Samuelson, A. G. *Indian J. Exp. Biol.* **1997**, 810–814.
(27) Berners-Price, S. J.; Johnson, R. K.; Mirabelli, C. K.; Faucette, L. F.; McCabe, F. L.; Sadler, P. J. *Inorg. Chem.* **1987**, *26*, 3383–3387.
(28) Berners-Price, S. J.; Sadler, P. J. *Struct. Bonding (Berlin)* **1988**, *70*, 27–102.
(29) Marzano, C.; Pellei, M.; Alidori, S.; Brossa, A.; Lobbia, G. G.; Tisato, F.; Santini, C. *J. Inorg. Biochem.* **2006**, *100*, 299–304.
(30) Rankin, G. O. *J. Toxicol. Environ. Health, Part B* **2004**, *46*, 5486–5489.
(31) Phosphacreatine is a P−N-bond-containing compound synthesized in the liver and transported to the muscle cells for storage, which can readily generate ATP from ADP on demand within 2−7 s.
(32) Priya, S.; Balakrishna, M. S.; Mague, J. T.; Mobin, S. M. *Inorg. Chem.* **2003**, *42*, 1272–1281.
(33) (a) Balakrishna, M. S.; Eisler, D.; Chivers, T. *Chem. Soc. Rev.* **2007**, *36*, 650–664. (b) Suresh, D.; Balakrishna, M. S.; Mague, J. T. *Dalton Trans.* **2008**, 3272–3274. (c) Chandrasekaran, P.; Mague, J. T.; Balakrishna, M. S. *Organometallics* **2005**, *24*, 3780–3783. (d) Chandrasekaran, P.; Mague, J. T.; Balakrishna, M. S. *Inorg. Chem.* **2005**, *44*, 7925–7932. (e) Chandrasekaran, P.; Mague, J. T.; Balakrishna, M. S. *Inorg. Chem.* **2006**, *45*, 5893–5897. (f) Chandrasekaran, P.; Mague, J. T.; Balakrishna, M. S. *Inorg. Chem.* **2006**, *45*, 6678–6683. (g) Chandrasekaran, P.; Mague, J. T.; Balakrishna, M. S. *Dalton Trans.* **2009**, 5478–5486. (h) Chandrasekaran, P.; Mague, J. T.; Venkateswarn, R.; Balakrishna, M. S. *Eur. J. Inorg. Chem.* **2007**, 4998–4997. (i) Balakrishna, M. S.; Venkateswarn, R.; Mague, J. T. *Inorg. Chem.* **2009**, *48*, 1398–1406. (j) Balakrishna, M. S.; Chandrasekaran, P.; Venkateswarn, R. *J. Organomet. Chem.* **2007**, *692*, 2642–2648. (k) Balakrishna, M. S.; Mague, J. T.; Chandrasekaran, P. *Dalton Trans.* **2007**, 2957–2962.
(34) Suresh, D.; Balakrishna, M. S.; Rathinasamy, K.; Panda, D.; Mobin, S. M. *Dalton Trans.* **2008**, 2812–2814.
(35) Suresh, D.; Balakrishna, M. S.; Rathinasamy, K.; Panda, D.; Mague, J. T. *Dalton Trans.* **2008**, 2285–2292.

Scheme 1. Preparation of Mixed-Ligand Copper(I) Complexes from Octanuclear Macrocycles

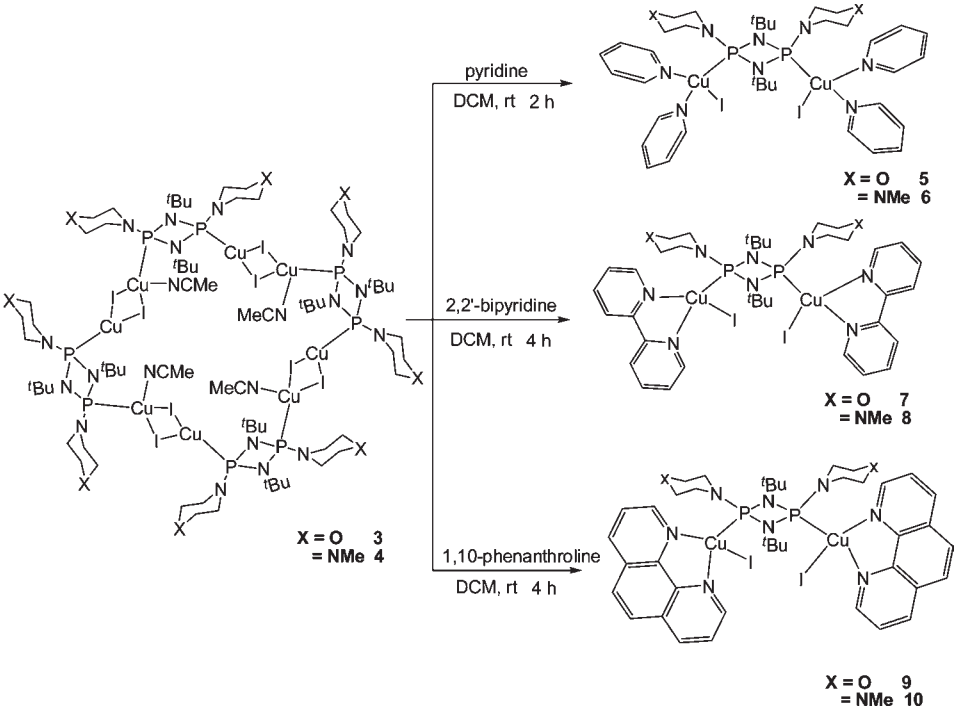

dichloromethane afforded the mixed-ligand complexes $[(C_5H_5N)_4Cu_2I_2\{[^tBuNP(NC_4H_8X)]_2\}]$ (**5**, X = O; **6**, X = NMe) in good yield. The $^{31}P\{^1H\}$ NMR spectra of complexes **5** and **6** show broad singlets at 71.3 and 71.4 ppm, respectively, which are shifted downfield from that of the metallmacrocycles ($\delta_P \sim 69$ ppm). The slow addition of 2 equiv of 2,2′-bipyridine and 1,10-phenanthroline to 1 equiv of **3** or **4** in dichloromethane at room temperature resulted in the formation of neutral dinuclear complexes $[(2,2'\text{-bpy})_2Cu_2I_2\{[^tBuNP(NC_4H_8X)]_2\}]$ (**7**, X = O; **8**, X = NMe) and $[(1,10\text{-phen})_2Cu_2I_2\{[^tBuNP(NC_4H_8X)]_2\}]$ (**9**, X = O; **10**, X = NMe) as yellow crystalline solids (Scheme 1). The $^{31}P\{^1H\}$ NMR spectra of complexes **7** and **8** show broad singlets, respectively, at 75.9 and 75.2 ppm, whereas those of complexes **9** and **10** also show single resonances at 74.7 and 77.6 ppm, respectively. The ^1H NMR spectra and microanalytical data for complexes **5**−**10** agree well with the proposed structures. The molecular structures of complexes **9** and **10** were confirmed by single-crystal X-ray diffraction studies.

Molecular Structures of Complexes 9 and 10. Perspective views of the molecular structures of complexes **9** and **10** along with their atom labeling schemes are shown in Figures 1 and 2. The crystallographic data and details of the structure determination are given in Table 1, while selected bond lengths and bond angles are listed in Tables 2 and 3. The yellow crystals of complex **9** suitable for single-crystal X-ray diffraction studies were obtained by the slow evaporation of a dichloromethane/acetonitrile solution at room temperature. The mixed-ligand complex **9** crystallized with one unique molecule of acetonitrile in the lattice. The amido $[-N(CH_2)_4O)]$ groups are in chair conformations and are in a mutually cis disposition on the P_2N_2 ring. The phosphorus atom of the cyclodiphosphazane ligand, the two nitrogen atoms of the phenanthroline ligand, and one iodine atom comprise the coordination

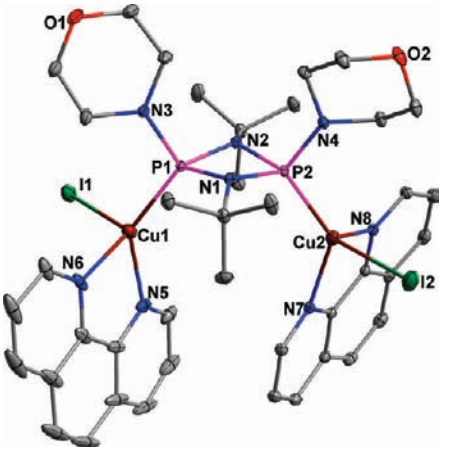

Figure 1. Diamond view of molecular structure of **9**. All hydrogen atoms and the lattice acetonitrile were omitted for clarity. Thermal ellipsoids are drawn at the 50% probability level.

spheres of the copper(I) centers (Cu1 and Cu2), which adopt a distorted tetrahedral geometry. The largest deviation from the ideal geometry is in the N5−Cu1−N6 and P1−Cu1−N5 bond angles of 79.55(7)° and 134.19(5)°, respectively [for Cu2, N7−Cu2−N8 = 80.02(6)° and P2−Cu2−N7 = 129.64(4)°], which are markedly different from the perfect tetrahedral value of 109.4°. The Cu−P [Cu1−P1 = 2.2033(5) Å and Cu2−P2 = 2.1915(5) Å] bond lengths are similar and are longer than the same ones in the tetranuclear mixed-ligand complex $\{[\{P(\mu\text{-}NC_5H_4\text{-}N)\}_2(\mu\text{-}O)]_2[CuCl(C_5H_5N)_2]_4\}$[36] [P1−Cu1 = 2.1482(8) Å and P2−Cu2 = 2.1308(9) Å]. The Cu−N bond distances vary from 2.0795(15) Å (Cu2−N7) to 2.1303(18) Å (Cu1−N6). The average Cu−I bond lengths are 2.676 Å.

(36) Bond, A. D.; Doyle, E. L.; Garcia, F.; Kowenicki, R. A.; McPartlin, M.; Riera, L.; Wright, D. S. *Chem. Commun.* **2003**, 2990.

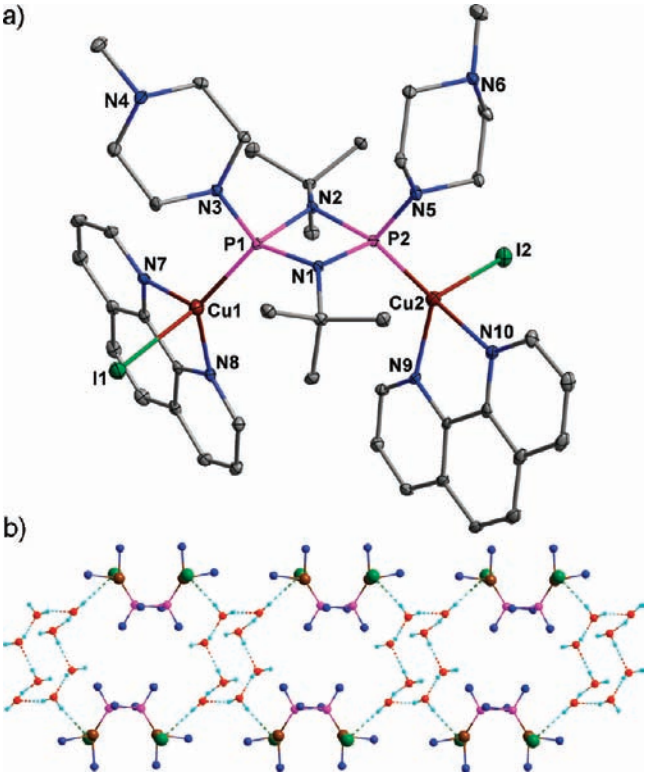

Figure 2. (a) Diamond view of molecular structure of **10**. All hydrogen atoms and the lattice water and acetonitrile were omitted for clarity. Thermal ellipsoids are drawn at the 50% probability level. (b) Ball-and-stick model of the molecular structure of **10** showing the hydrogen-bonding network. All hydrogen atoms (except OH), ^{t}Bu groups, 1,10-phen groups, piperazine moieties, and lattice acetonitrile were omitted for clarity.

Table 1. Crystallographic Data for Complexes **9** and **10**

	9·CH_3CN	**10**·CH_3CN·$4H_2O$
formula	$C_{42}H_{52}Cu_2I_2N_9O_2P_2$	$C_{44}H_{67}Cu_2I_2N_{11}O_4P_2$
fw	1158.75	1256.91
cryst syst	monoclinic	triclinic
space group	$P2_1/c$ (No. 14)	$P\bar{1}$ (No. 2)
a, Å	18.981(1)	12.609(1)
b, Å	10.187(1)	14.843(1)
c, Å	25.673(1)	14.939(1)
α, deg	90	103.025(1)
β, deg	98.252(1)	92.238(1)
γ, deg	90	107.422(1)
V, Å^3	4912.8(3)	2582.0(3)
Z	4	2
ρ_{calc}, g/cm^3	1.567	1.617
μ(Mo Kα), mm^{-1}	2.231	2.133
F(000)	2312	1268
cryst size, mm^3	0.18 × 0.21 × 0.22	0.07 × 0.12 × 0.13
T, K	100	100
2θ range, deg	1.6, 28.0	2.1, 28.3
total no. of reflns	42 242	28 663
no. of indep reflns	11 597 (R_{int} = 0.026)	22 244 (R_{int} = 0.063)
R1[a]	0.0223	0.0372
wR2[b]	0.0547	0.0868
GOF (F^2)	1.033	1.070

[a] $R = \sum||F_o| - |F_c||/\sum|F_o|$. [b] $wR2 = \{[\sum w(F_o^2 - F_c^2)/\sum w(F_o^2)^2]\}^{1/2}$, $w = 1/[\sigma^2(F_o^2) + (xP)^2]$, where $P = (F_o^2 + 2F_c^2)/3$.

The shortest Cu···Cu distance is 5.124 Å, which is well beyond the van der Waals radii, eliminating any possible metal−metal interaction.

The dinuclear copper(I) complex **10** has a structure basically the same as that of **9** and crystallizes with one unique molecule of acetonitrile and four molecules of water in the lattice. The presence of strong hydrogen bonding between the four water molecules (O1−H1OB···O2, O2−H2OB···O3, O3−H3OA···O4, O3−H3OB···O4, and O4−H4OB···O1) leads to the formation water clusters. The intermolecular hydrogen bonding further extends to the iodide (Cu−I) and the hydrogen atom of the water molecule (O1−H1OA···I1 and O2−H2OA···I2), which, in turn, forms a one-dimensional polymeric sheetlike structure, as shown in Figure 2b. The patterns of other bond lengths and bond angles in **10** are similar to those in **9**.

Table 2. Selected Bond Lengths (Å) and Bond Angles (deg) for **9**

bond	length (Å)	bond	angle (deg)
I1−Cu1	2.6756(3)	I1−Cu1−P1	110.65(1)
I2−Cu2	2.6761(3)	I1−Cu1−N5	97.04(5)
Cu1−P1	2.2033(5)	I1−Cu1−N6	107.36(5)
Cu1−N5	2.0824(17)	P1−Cu1−N5	134.19(5)
Cu1−N6	2.1303(18)	P1−Cu1−N6	122.45(5)
Cu2−P2	2.1915(5)	N5−Cu1−N6	79.55(7)
Cu2−N7	2.0795(15)	I2−Cu2−P2	117.69(1)
Cu2−N8	2.1062(15)	I2−Cu2−N7	98.75(4)
P1−N1	1.7265(15)	I2−Cu2−N8	101.17(4)
P1−N2	1.7084(16)	P2−Cu2−N7	129.64(4)
P1−N3	1.6654(16)	P2−Cu2−N8	80.02(6)
		Cu1−P1−N2	124.05(6)
		Cu1−P1−N3	109.75(6)

Table 3. Selected Bond Lengths (Å) and Bond Angles (deg) for **10**

bond	length (Å)	bond	angle (deg)
I1−Cu1	2.7006(7)	I1−Cu1−P1	118.65(3)
I2−Cu2	2.6452(5)	I1−Cu1−N7	102.66(8)
Cu1−P1	2.1953(11)	I1−Cu1−N8	94.01(8)
Cu1−N7	2.110(4)	P1−Cu1−N7	118.88(9)
Cu1−N8	2.083(3)	P1−Cu1−N8	133.71(10)
Cu2−P2	2.1902(11)	N7−Cu1−N8	80.11(13)
Cu2−N9	2.055(3)	I2−Cu2−P2	121.83(3)
Cu2−N10	2.134(4)	I2−Cu2−N9	100.07(8)
P1−N1	1.724(4)	I2−Cu2−N10	102.85(8)
P1−N2	1.707(3)	P2−Cu2−N9	128.22(9)
P1−N3	1.674(3)	P2−Cu2−N10	114.25(9)
O1−H1OA···I1	2.7200	N9−Cu2−N10	80.27(13)
O2−H2OA···I2	2.8000	Cu1−P1−N1	121.74(11)
O1−H1OB···O2	1.9400	Cu1−P1−N2	124.25(12)
O2−H2OB···O3	1.9600	Cu1−P1−N3	109.99(12)
O3−H3OA···O4	2.0400	O1−H1OA···I1	170.00
O3−H3OB···O4	2.0200	O2−H2OA···I2	172.00
O4−H4OB···O1	1.9600	O1−H1OB···O2	161.00
		O2−H2OB···O3	164.00
		O3−H3OA···O4	158.00
		O3−H3OB···O4	157.00
		O4−H4OB···O1	154.00

Antiproliferative Properties of Copper Complexes 3, 5, and 7−9. We examined the antiproliferative activity of five different dinuclear copper(I) complexes, **3**, **5**, and **7**−**9**, using human cervical cancer (HeLa) cells in culture. These complexes showed varied levels of antiproliferative activities against HeLa cells (Table 4).

Of all of the compounds tested, the 1,10-phenanthroline derivative, [(1,10-phen)$_2$Cu$_2$I$_2${[^{t}BuNP(NC$_4$H$_8$O)]$_2$}] (**9**), displayed higher antiproliferative activity than the other compounds. Therefore, we sought to investigate the antiproliferative mechanism of action of complex **9** in detail.

Complex **9** inhibited the proliferation of HeLa, human breast cancer cells (MCF-7), and highly metastatic breast

cancer cells (MDA-MB 231) in a concentration-dependent manner (Figure 3a−c). Half-maximal inhibitory concentration (IC_{50}) values were determined to be 2.7 ± 0.2, 2.8 ± 0.6, and 1.25 ± 0.25 μM for HeLa, MCF-7, and MDA-MB 231cells, respectively. The antiproliferative effects of cisplatin on HeLa, MCF-7, and MDA-MB 231 cells were also determined under similar conditions. 50% inhibition of HeLa, MCF-7, and MDA-MB 231 cells occurred in the presence of 10, 15, and 20 μM cisplatin, respectively. The results suggest that complex **9** is a more potent inhibitor of various types of cancer cells in culture than cisplatin, a widely used antitumor agent.

Table 4. Copper Complexes Inhibiting Proliferation of HeLa Cells

complex	% inhibition at 1 μM	% inhibition at 5 μM	% inhibition at 10 μM
3	26 ± 3	39 ± 2	62 ± 9
5	12 ± 3	29 ± 6	50 ± 4
7	15 ± 5	29 ± 6	43 ± 5
8	12 ± 3	20 ± 8	34 ± 7
9	21 ± 6	97 ± 6	100
cisplatin			49 ± 7

Complex **9** also inhibited the proliferation of Chinese hamster ovary (CHO) cells, a nontransformed cell line, with an IC_{50} of 4.10 ± 0.4 μM (Figure 3d), while 20 μM cisplatin inhibited proliferation of CHO cells by ~40%.

Complex 9 Blocking Cell Cycle Progression in the G1 Phase and Inducing Apoptosis. We examined the effect of complex **9** on the cell cycle progression of MCF-7 cells using fluorescence activated cell sorting (FACS). Treatment with complex **9** caused an increase in the number of MCF-7 cells in the G1 phase (Figure 4). For example, 47% of the control cells (vehicle treated) were found to be in the G1 phase, while 67% and 89% of the cells were in the G1 phase when the cells were incubated with 6 μM (~2IC_{50}) of complex **9** for 24 and 48 h, respectively. Treatment with complex **9** also resulted in an increase in the sub-G0 phase from 4% in the control to 58% in the 6 μM complex **9** (~2IC_{50}) after 48 h of the cell cycle, suggesting that complex **9** reduced the viability of the cells (Table 5).

Immunostaining with a cyclin B1 (specific for the G2/M phase) antibody showed that there was no increase in the

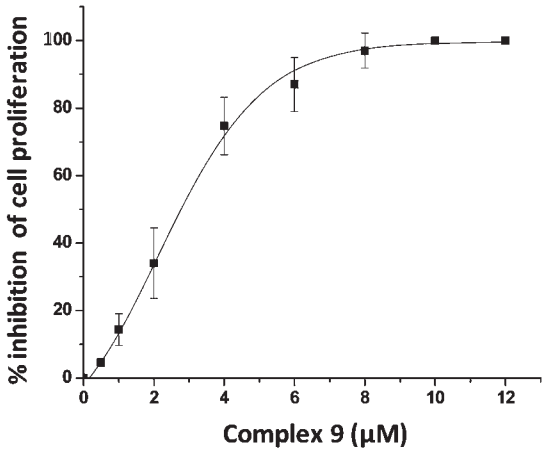

a. Half maximal inhibitory concentration (IC_{50}) for MCF-7 cells = 2.8 ± 0.6 μM

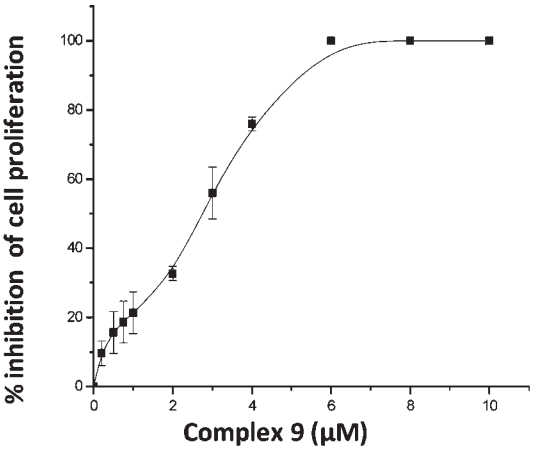

b. Half maximal inhibitory concentration (IC_{50}) for HeLa cells = 2.7 ± 0.2 μM

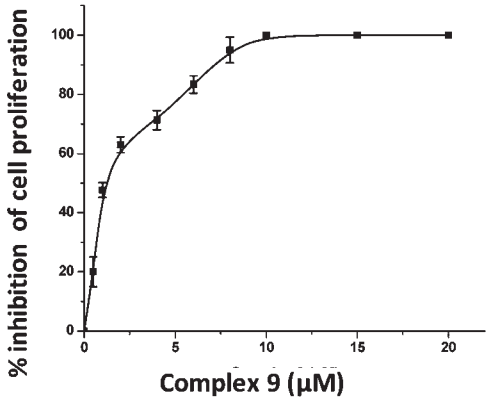

c. Half maximal inhibitory concentration (IC_{50}) for MDA-MB 231 cells = 1.25 ± 0.25 μM

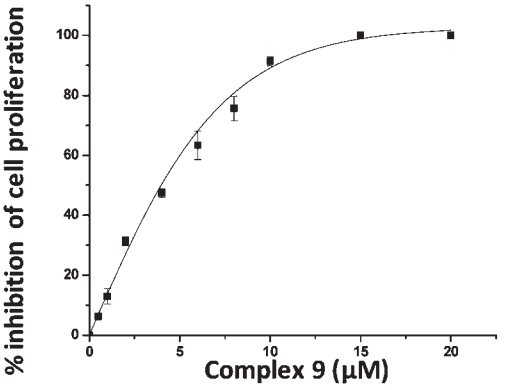

d. Half maximal inhibitory concentration (IC_{50}) for CHO cells = 4.1 ± 0.4 μM

Figure 3. Complex **9** inhibited proliferation of MCF-7 (a), HeLa (b), MDA-MB 231 (c), and CHO (d) cells. % inhibition of cell proliferation was determined using sulforhodamine B assay.

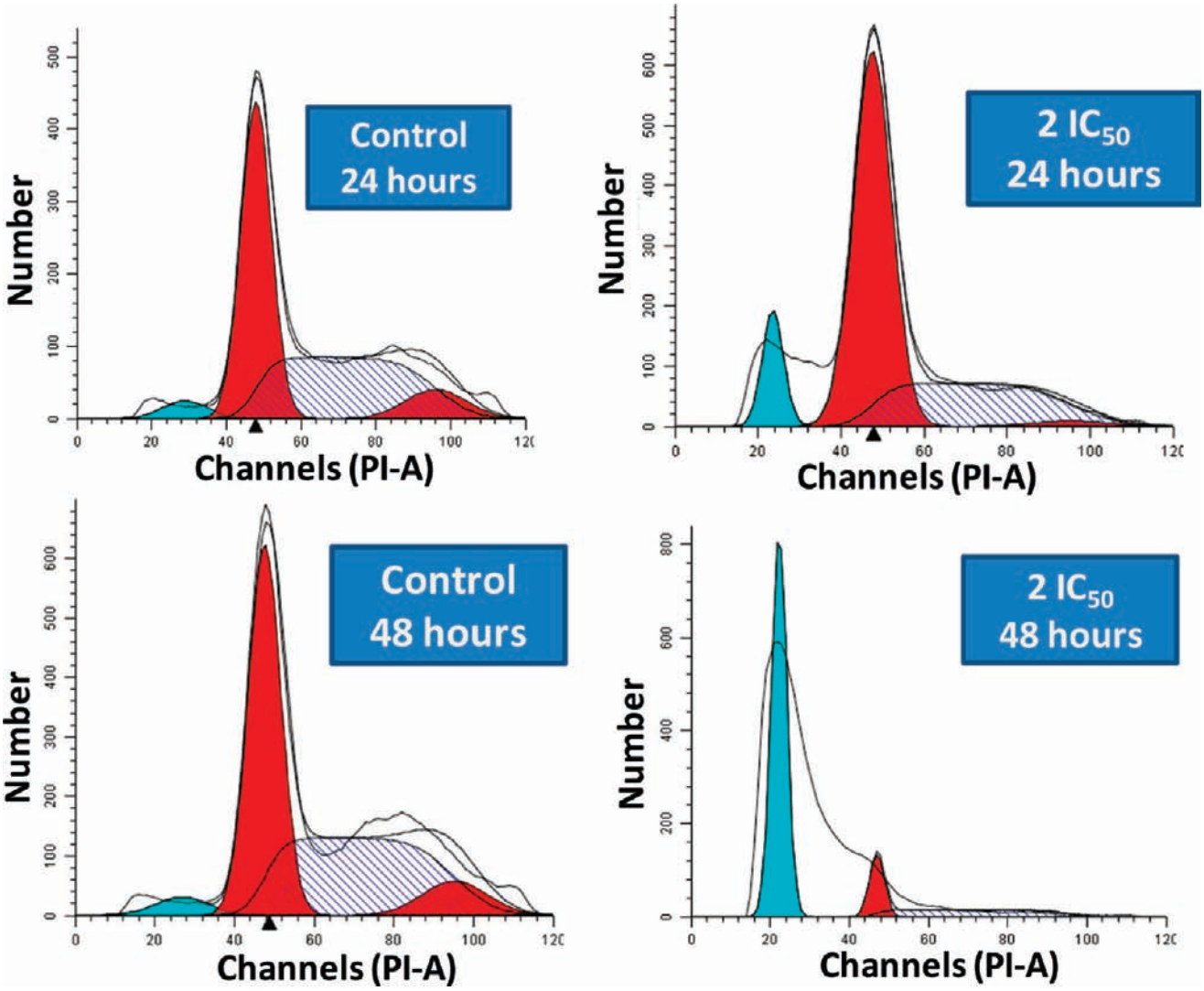

Figure 4. Flow cytometry analysis showing complex **9** blocked MCF-7 cells in the G1 phase of the cell cycle. The DNA content of the samples was determined by FACS analysis. The red color in the histograms shows the percentage of cells stained with PI present in the G1 and G2/M phases of the cell cycle. The blue color in the histograms shows the percentage of cells in apoptosis.

expression of cyclin B1, suggesting that complex **9** does not block cells in the G2/M phase (data not shown).

Because FACS data showed that complex **9** leads to a block in the cell cycle and a decrease in the cell viability, we examined whether complex **9** induced apoptosis in MCF-7 cells using Annexin V and propidium iodide (PI) staining. Vehicle-treated cells did not show Annexin/PI staining, while cells treated with complex **9** showed Annexin V and PI staining, indicating that complex **9** induced cell death via apoptosis (Figure 5).

We also performed DNA fragmentation assays to further confirm the apoptotic cell death. During apoptosis, endonuclease is known to cleave the nucleosomes, which leads to the generation of DNA fragments (48). In control MCF-7 cells, genomic DNA was intact and showed a single band; however, cells treated with complex **9** showed fragmented DNA, indicating that complex **9** induced cell death via apoptosis (Figure 6).

Because complex **9** inhibited the proliferation of various cells in culture and caused apoptosis, we examined the pathway by which complex **9** induced apoptosis. MCF-7 cells were incubated in the absence or presence of complex **9** for 24 h and then stained with Hoechst 33258. Complex **9** strongly affected the DNA integrity (Figure 7). In control interphase cells, the nucleus was well compact, whereas the treatment with complex **9** disorganized the nucleus and induced the degradation of DNA. In complex **9**-treated interphase cells, DNA appeared to be granular instead of compact. In control mitotic cells, the chromosomes were aligned properly on the metaphase plate, whereas the cells treated with complex **9** showed puffy chromosomes (Figure 7). Complex **9** exerted similar effects in HeLa cells (data not shown).

Table 5. Complex **9** Inhibiting the Progression of the MCF-7 Cells in the G1 Phase and Inducing Apoptosis

	% of cells in the phase			
	G1	S	G2/M	apoptosis
control (24 h)	47 ± 3	44 ± 2	9 ± 1	4 ± 1
$2IC_{50}$ (24 h)	67 ± 5	31 ± 3	2 ± 1	10 ± 2
control (48 h)	47 ± 1	45 ± 3	8 ± 3	3 ± 1
$2IC_{50}$ (48 h)	89 ± 3	7 ± 2	4 ± 1	58 ± 3

Complex 9 Inducing Nuclear Localization of Tumor Suppressor Protein p53. Complex **9** disturbed the DNA

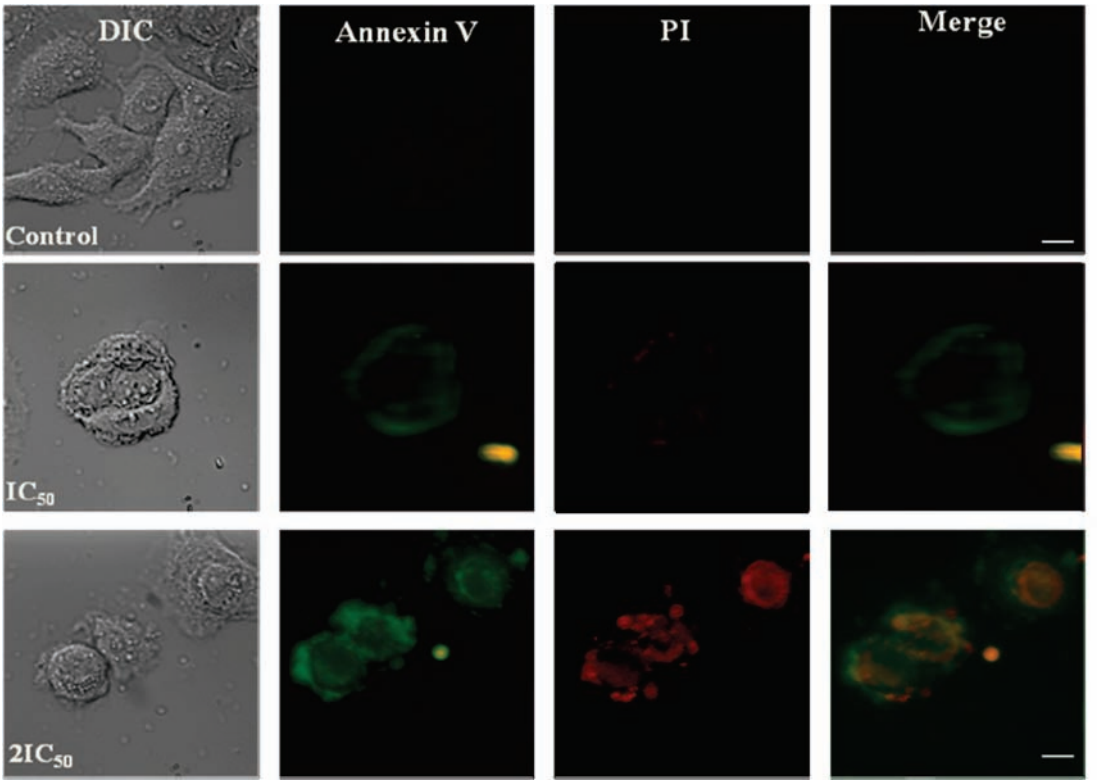

Figure 5. Annexin V (green) and PI (red) staining showing early and late stages of apoptosis after the treatment of MCF-7 cells with complex **9**. The scale bar is 10 μm.

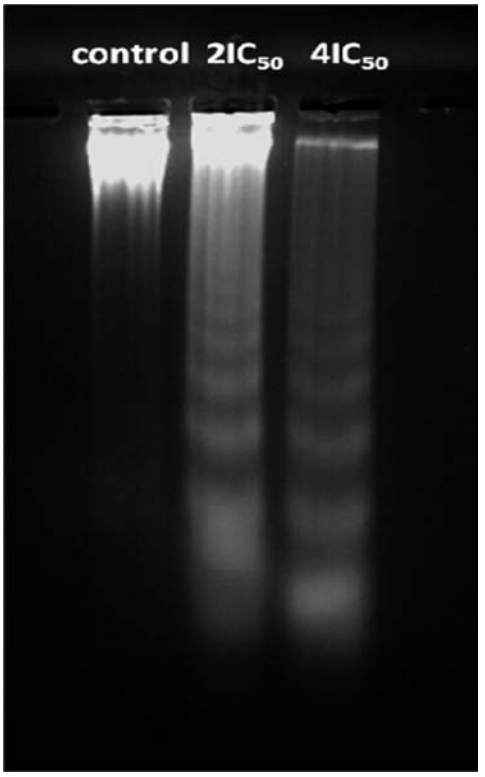

Figure 6. DNA band analysis by UV gel doc. Complex **9** treatment induced DNA fragmentation in MCF-7 cells. MCF-7 cells were incubated without and with complex **9** ($2IC_{50}$ and $4IC_{50}$) for 48 h.

integrity and induced apoptosis; therefore, we examined its effect on the nuclear localization of p53. MCF-7 cells contain wild-type p53. We used GFP-p53 transfected MCF-7 cells to examine the effects of complex **9** on the nuclear localization of p53 and its downstream products. The complex **9** treatment increased the nuclear localization of GFP-p53 in MCF-7 cells in a concentration-dependent manner (Figure 8). The proportion of cells having GFP-p53 inside the nucleus in control cells was 7% and in 6 μM complex **9** ($\sim 2 \times IC_{50}$) treated cells it was 71% (Table 6). Similar results were obtained with indirect immunostaining of p53 using an antibody against p53. For example, vehicle treated MCF-7 cells did not show p53 staining, while in the presence of 6 μM complex **9** ($\sim 2IC_{50}$) most of the MCF-7 cells showed nuclear accumulation of p53 (Figure 8b).

The key regulator of the p53 pathway is its downstream gene p21. Therefore, the effect of complex **9** on the nuclear accumulation of p21 was examined in MCF-7 cells. The agent increased the expression and localization of p21 inside the nucleus (Figure 9). In control cells, 3% of cells showed p21 localization inside the nucleus, while 6 μM complex **9** ($\sim 2IC_{50}$) treated cells showed 54% of p21 inside the nucleus (Table 6).

In order to know whether the activities are inherent properties of the complexes or the individual components either in isolated form or in combination, we studied the interactions of various components present in complex **9**. Complex **9** in 5 μM concentration inhibited HeLa cell proliferation by 97%, whereas none of the components inhibited HeLa cell proliferation under this condition. Even at 10 μM concentration, cyclodiphosphazane **1**, 2′-bipyridine, 4,4′-bipyridine, 1,10 phenanthraline, and pyridine inhibited HeLa cell proliferation by 17 ± 2, 20 ± 2, 18 ± 1, 10 ± 3, and 15 ± 3%, respectively. This clearly

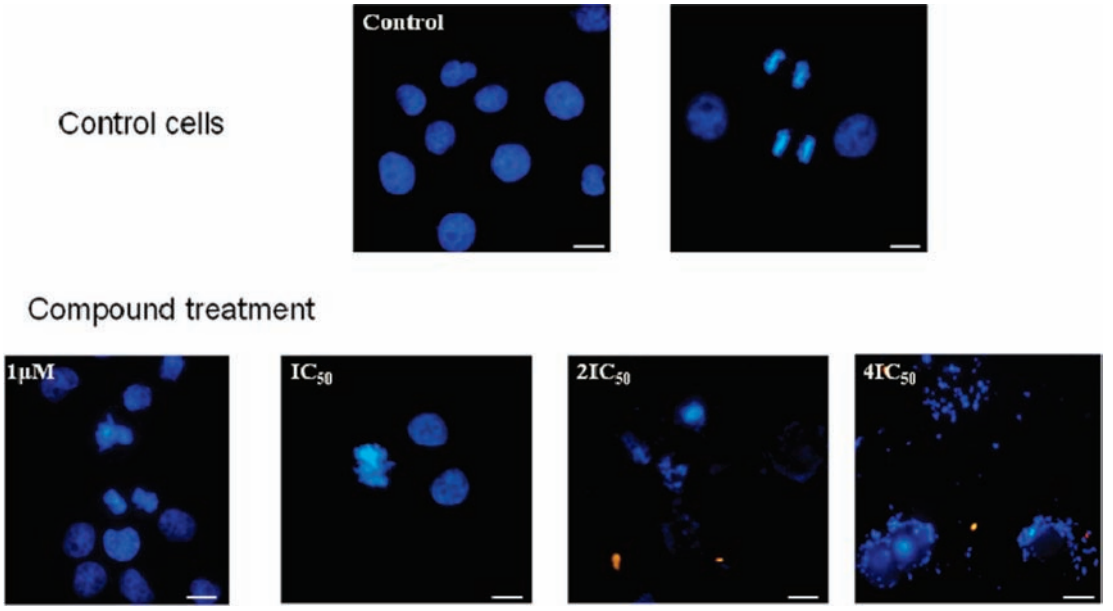

Figure 7. Complex **9** perturbing the DNA integrity in MCF-7 cells. MCF-7 cells were incubated without and with different concentrations of complex **9** for 24 h. After incubation with complex **9**, cells were fixed as described in methodology and stained with Hoechst 33258 (blue in color) to visualize the DNA morphology of the cells. The scale bar is 10 μm.

demonstrates that the individual components do not show cytotoxicity. Further, the free ligand **1** and complex **9** are stable in biological media for several hours and show little or no degradation even after 10 h, indicating that the mixed-ligand complex stays intact during proliferation, as verified from ^{31}P NMR data. In view of this, further mechanistic investigations are essential to fully understanding the detailed molecular mechanism of cytotoxicity.

Conclusions

Cisplatin, carboplatin, and other platinum-based antitumor drugs are highly active toward testicular cancers and are also effective against a wide range of other tumors such as ovarian, bladder carcinoma, and non-small-cell lung cancer. However, treatment failure is often caused by the development of resistance to these complexes and is also due to their high nephrotoxicity and neurotoxicity. Interestingly, copper has not been shown to cause cancer in human beings or in animals, and the international agency for research on cancer has not classified copper as a human carcinogen. Further, copper deficiency can result in increased in plasma and LDL cholesterol, and a decrease in HDL cholesterol leads to the possibility of cardiovascular attack, increased cellular oxidation, more lipid oxidation, obesity, graying of hair, increased sensitivity to pain, accelerated development of Alzheimer's disease, and also reproductive problems.

The presence of copper with a daily intake not exceeding 4−7 mg is safe and can minimize the above-mentioned diseases. Therefore, it is appropriate to design anticancer drugs based on copper, which is anticipated to cause lower toxic effects. In this context, we have developed several mixed-ligand complexes of copper(I) that are expected to be less toxic but highly potent in smaller dosage compared to cisplatin and analogous compounds.

Complex **9** displayed potent antiproliferative activity against several types of cancer cells in culture. The effect of complex **9** was studied on the nontransformed cell line CHO, and its effect was found to be less on CHO cells compared to that on highly metastatic breast cancer cells. Thus, on the basis of antiproliferative activity, we suggest that complex **9** may have some specificity against cancer cells. Under similar conditions, complex **9** displayed several-fold stronger antiproliferative activity against different types of cancer cells than cisplatin, suggesting that complex **9** has a strong chemotherapeutic potential. A study of its mechanism of action showed that complex **9** affected the DNA integrity in both HeLa and MCF-7 cells, blocked the MCF-7 cells in the G1 phase of the cell cycle, and induced apoptosis via a p53-dependent apoptotic pathway.

Presently, we are focusing on understanding the type of interaction between the copper complexes and DNA that is responsible for the cytotoxicity.

Experimental Section

General Procedures. All experimental manipulations were carried out under a dry nitrogen or argon atmosphere, using standard Schlenk techniques unless otherwise stated. Solvents were dried and distilled prior to use by conventional methods. The precursor complexes $[Cu_8(\mu_2\text{-}I)_8(CH_3CN)_4(\mu\text{-}N^tBuP)_8(NC_4H_8NMe)_8]$ (**3**, X = O; **4**, NMe) were prepared according to published procedures.[33b] All pyridyl derivatives were purchased from Aldrich and were used without further purification.

Spectroscopy. The ^{1}H and ^{31}P{^{1}H} NMR (δ in ppm) spectra were obtained on a Varian VXR 400 spectrometer operating at frequencies of 400 and 162 MHz, respectively. Tetramethylsilane and 85% H_3PO_4 were used as internal and external standards for ^{1}H and ^{31}P{^{1}H} NMR, respectively. Positive shifts lie downfield of the standard in all cases. Microanalyses were carried out on a Carlo Erba model 1106 elemental analyzer. Melting points of all complexes were determined on a Veego melting point apparatus and were uncorrected.

Synthesis of $[(C_5H_5N)_4Cu_2I_2\{[^tBuNP(NC_4H_8O)]_2\}]$ (5). A solution of pyridine (2 mL) in dichloromethane (5 mL) was added dropwise to **3** (0.040 g, 0.051 mmol) in dichloromethane (8 mL) at room temperature, and the reaction mixture was allowed to stir at room temperature for 3 h. All of the volatiles were removed under vacuum, and the residue was dissolved in dichloromethane, layered with petroleum ether, and stored at −30 °C to give yellow

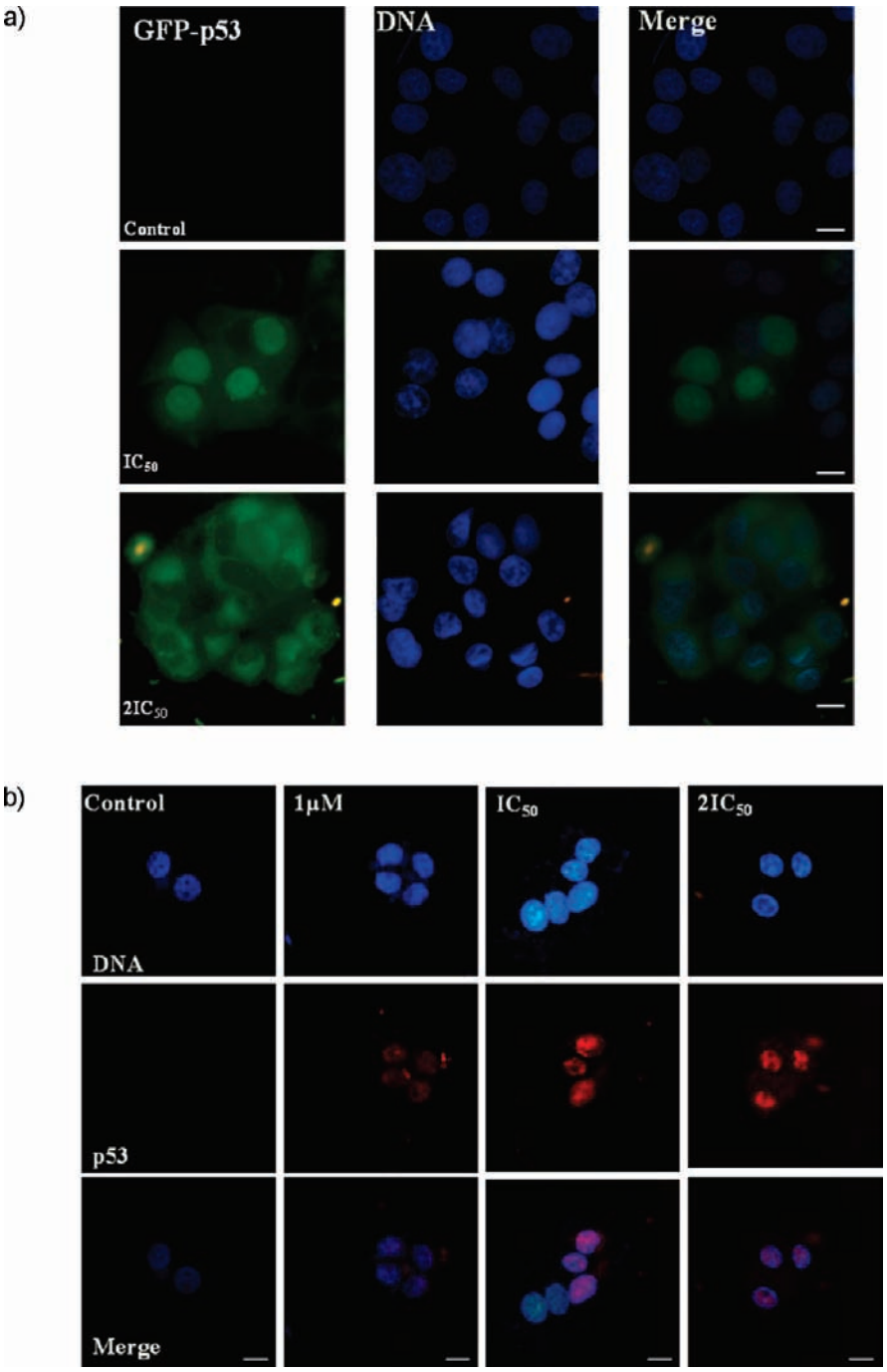

Figure 8. Complex **9** treatment enhancing the expression and nuclear localization of p53 in MCF-7 cells. MCF-7 cells were incubated without and with different concentrations of complex **9** for 24 h: (a) localization of GFP-tagged p53 (green in color) observed under a microscope; (b) Cells fixed and immunostaining performed using an antibody specific for p53 (red). The nucleus was stained with Hoechst 33258 (blue). The scale bar is 10 μm.

crystals of **5**. Yield: 70% (0.038 g, 0.036 mmol). Mp: 166−170 °C (dec). Anal. Calcd for $C_{36}H_{54}N_8O_2P_2Cu_2I_2$: C, 40.27; H, 5.07; N, 10.44. Found: C, 40.43; H, 5.15; N, 10.37. ^{1}H NMR (400 MHz, $CDCl_3$, δ): 7.72−7.33 (m, *Py*, 20H), 3.66 (br s, CH_2, 16H), 1.45 (s, ^{t}*Bu*, 18H). ^{31}P{^{1}H} NMR (161.8 MHz, $CDCl_3$, δ): 71.3 (br s).

Synthesis of $[(C_5H_5N)_4Cu_2I_2\{[^t$BuNP$(NC_4H_8$NMe$)]_2\}]$ (6). This compound was synthesized by a procedure similar to that of **5**, using **4** (0.039 g, 0.051 mmol) and pyridine (2 mL). Yield: 72% (0.041 g, 0.037 mmol). Mp: 140−142 °C (dec). Anal. Calcd for $C_{38}H_{60}N_{10}P_2Cu_2I_2$: C, 41.50; H, 5.50; N, 12.74. Found: C, 41.62; H, 5.38; N, 12.65. ^{1}H NMR (400 MHz, $CDCl_3$, δ): 7.72−7.69 (m, *Py*, 20H), 3.58 (br s, CH_2, 8H), 3.27 (br s, CH_2 8H), 2.34 (br s, *NMe*, 6H), 1.43 (s, ^{t}*Bu*, 18H). ^{31}P{^{1}H} NMR (161.8 MHz, $CDCl_3$, δ): 71.4 (br s).

Synthesis of $[(2,2'$-bpy$)_2Cu_2I_2\{[^t$BuNP$(NC_4H_8O)]_2\}]$ (7). To solution of **3** (0.040 g, 0.051 mmol) in dichloromethane (5 mL) was added dropwise a solution of 2,2′-bipyridine (0.016 g, 0.102 mmol) in the same solvent (5 mL) at room temperature. The reaction mixture was allowed to stir for a further 6 h, concentrated to 4 mL, and layered with petroleum ether (2 mL). The clear yellow solution was stored at room temperature for 48 h to obtain **3** as yellow-orange crystals. Yield: 72% (0.039 g, 0.037 mmol). Mp: 156−158 °C (dec). Anal. Calcd for $C_{36}H_{50}Cu_2I_2N_8O_2P_2$: C, 40.42; H, 4.71; N, 10.48. Found: C, 40.35; H, 4.55; N, 10.33. ^{1}H NMR (400 MHz, $CDCl_3$, δ): 7.96−7.36

(m, *bpy*, 16H), 3.58 (br s, CH_2, 16H), 1.56 (s, ^tBu, 18H). $^{31}P\{^1H\}$ NMR (161.8 MHz, $CDCl_3$, δ): 75.9 (s).

Synthesis of $[(2,2'\text{-bpy})_2Cu_2I_2\{[^t\text{BuNP}(NC_4H_8NMe)]_2\}]$ (8). This was synthesized by a procedure similar to that of **7**, using **4** (0.039 g, 0.051 mmol) and 2,2′-bipyridine (0.016 g, 0.102 mmol). Yield: 65% (0.036 g, 0.033 mmol). Mp: 178−182 °C (dec). Anal. Calcd for $C_{38}H_{56}N_{10}P_2Cu_2I_2$: C, 41.65; H, 5.15; N, 11.60. Found: C, 41.69; H, 5.10; N, 11.57. ^1H NMR (400 MHz, $CDCl_3$, δ): 7.96−7.36 (m, *bpy*, 16H), 3.49 (br s, CH_2, 16H), 2.24 (br s, *NMe*, 6H), 1.54 (s, ^tBu, 18H). $^{31}P\{^1H\}$ NMR (161.8 MHz, $CDCl_3$, δ): 75.2 (s).

Synthesis of $[(1,10\text{-phen})_2Cu_2I_2\{[^t\text{BuNP}(NC_4H_8O)]_2\}]$ (9). This was synthesized by a procedure similar to that of **7**, using **3** (0.040 g, 0.051 mmol) and 1,10-phenanthroline (0.018 mg, 0.102 mmol). Yield: 79% (0.049 g, 0.041 mmol). Mp: 162−164 °C (dec). Anal. Calcd for $C_{40}H_{50}Cu_2I_2N_8O_2P_2$: C, 42.98; H, 4.51; N, 10.03. Found: C, 42.82; H, 4.59; N, 10.17. ^1H NMR (400 MHz, $CDCl_3$, δ): 8.65−7.79 (m, *phen*, 16H), 3.61 (br s, CH_2, 16H), 1.42 (s, ^tBu, 18H). $^{31}P\{^1H\}$ NMR (161.8 MHz, $CDCl_3$, δ): 74.7 (s).

Synthesis of $[(1,10\text{-phen})_2Cu_2I_2\{[^t\text{BuNP}(NC_4H_8NMe)]_2\}]$ (10). This compound was synthesized by a procedure similar to that of **7**, using **4** (0.039 g, 0.051 mmol) and 1,10-phenanthroline (0.018 mg, 0.102 mmol). Yield: 73% (0.043 g, 0.037 mmol). Mp: 172−174 °C (dec). Anal. Calcd for $C_{42}H_{56}N_{10}P_2Cu_2I_2$: C, 44.10; H, 4.93; N, 12.25. Found: C, 44.22; H, 4.85; N, 12.36. ^1H NMR (400 MHz, $CDCl_3$, δ): 8.45−7.81 (m, *phen*, 16H), 3.31 (br s, CH_2, 16H), 2.24 (br s, *NMe*, 6H), 1.62 (s, ^tBu, 18H). $^{31}P\{^1H\}$ NMR (161.8 MHz, $CDCl_3$, δ): 77.6 (s).

Table 6. Complex **9** Treatment Increasing the Nuclear Localization of p53 and p21 in MCF-7 Cells[a]

complex **9** (μM)	% of cells having p53 inside the nucleus	% of cells having p21 inside the nucleus
0	7 ± 1	3 ± 1
3	49 ± 3	35 ± 5
6	71 ± 4	54 ± 3

[a] A total of 500 cells per condition were counted for nuclear localization of p53, while 500, 450, and 350 cells were counted for p21 localization in the control (vehicle treated) and at 3 and 6 μM, respectively.

Materials. Hoechst 33258 was purchased from Sigma (St. Louis, MO). Anti-Mouse IgG−Alexa 568 conjugate was purchased from Invitrogen (Carlsbad, CA). Mouse monoclonal anti p53 IgG, mouse monoclonal anti p21 IgG, and an annexin V apoptosis detection kit were purchased from Santa Cruz Biotechnology (Santa Cruz, CA). All other reagents were of analytical grade.

Cell Culture. Human cervical cancer (HeLa), human breast cancer (MCF-7), and Chinese hamster ovary (CHO) cells were cultured in Eagle's minimal essential medium, which was supplemented with 10% fetal bovine serum, 2.2 g/L of sodium bicarbonate, and a 1% antibiotic antimycotic solution containing streptomycin, amphotericin B, and penicillin. (For MCF-7 cells, the medium was supplemented with 0.28 U/mL of insulin.) Metastatic breast cancer (MDA-MB 231) cells were grown in Leibovitz's 15 (L-15) medium, supplemented with 2.2 g/L of sodium bicarbonate. Cells were grown inside a CO_2 incubator (Sanyo, San Diego, CA) at 37 °C in a humidified atmosphere having 5% CO_2 and 95% air.

Determination of the Antiproliferative Activity of Dinuclear Copper Complexes. HeLa cells were seeded at a density of 1×10^5 cells/mL in a 96-well plate (Nunc, Roskilde, Denmark). Five different copper complexes (10 mM stock dissolved in dimethyl sulfoxide, DMSO) were diluted in a medium to keep the final DMSO concentration at 0.1% (v/v). After 24 h of seeding, HeLa cells were incubated for another 24 h without and with different concentrations (1, 5, and 10 μM) of the complexes. The antiproliferative activity was determined by standard sulforhodamine B assay.[37,38] Data obtained were the average of three independent experiments.

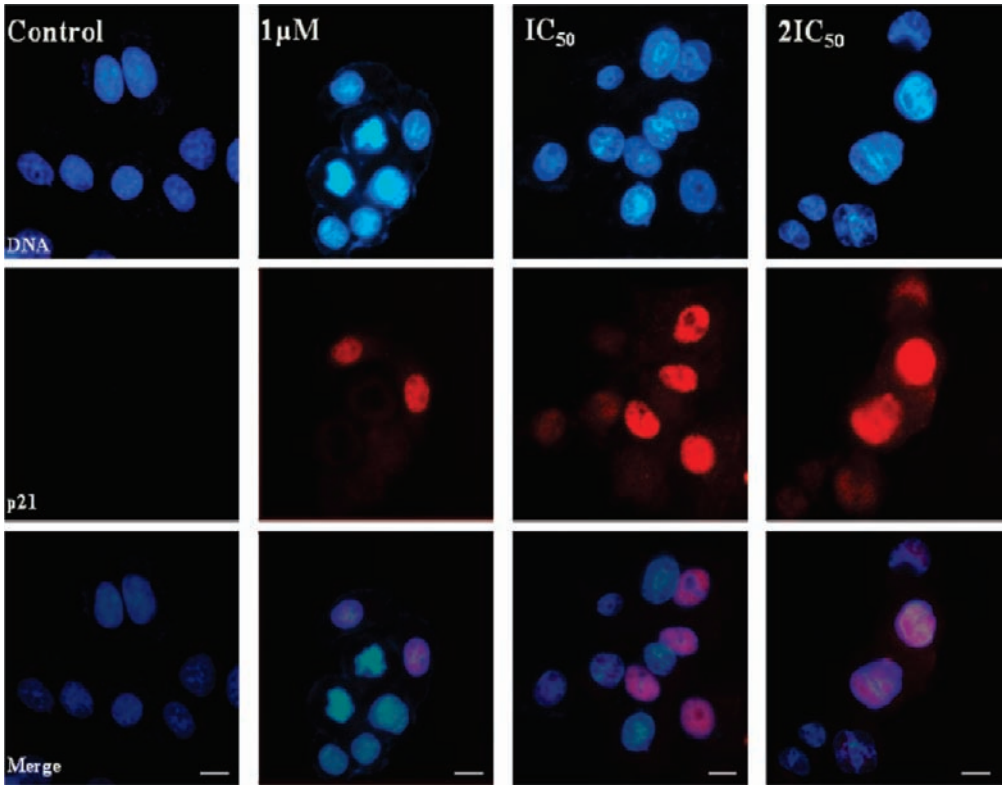

Figure 9. Complex **9** treatment activating the expression and nuclear localization of p21, a downstream protein in the p53 pathway in MCF-7 cells. MCF-7 cells were incubated without and with different concentrations of complex **9** for 24 h. Cells were fixed, and immunostaining was performed using an antibody specific for p21 (red). The nucleus was stained with Hoechst 33258 (blue). The scale bar is 10 μm.

To determine the half-maximal inhibitory concentration (IC_{50}) of complex **9**, HeLa, MCF-7, MDA-MB 231, and CHO cells were seeded at a concentration of 1×10^5 cells/mL in a 96-well plate for 24 h. Cells were grown in the absence or presence of different concentrations (ranging from 0.25 to 20 μM) of complex **9** for one cell cycle (24 h for HeLa, CHO, and MDA-MB 231 cells and 48 h for MCF-7 cells). The effect of complex **9** on the proliferation of cells was determined by a standard sulforhodamine B assay.[37,38] Data obtained were the average of three independent experiments. Experiments in MCF-7 cells were performed considering the IC_{50} value as 3 μM.

Cell Cycle Analysis Using FACS. Samples for flow cytometry were prepared as described.[39] Briefly, MCF-7 cells ($\sim 1 \times 10^6$ cells/mL) were incubated without or with 6 μM ($2IC_{50}$) complex **9** for either 24 or 48 h. Cells were trypsinized after 24 and 48 h of complex **9** treatment and centrifuged at 2000 rpm for 10 min at room temperature (25 °C). The cells were washed twice with phosphate-buffered saline (PBS) and fixed with 70% alcohol. After fixation, the cells were pelleted and washed twice with PBS and then further incubated with propidium iodide (PI; 50 μg/mL) and RNase (1 μg/mL) in ice for 2 h. The DNA contents of the control and complex **9** treated cells were quantified in a flow cytometer (FACS Aria Beckton Dickenson), and the cell cycle distribution was analyzed using the Modfit LT program (Verity Softwares, Topsham ME).

Annexin V/PI Staining. MCF-7 cells were incubated without or with complex **9** for 24 h and stained with Annexin V/PI as described recently.[39,40] Briefly, MCF-7 cells (0.5×10^5 cells/mL) were grown on polylysine-coated glass coverslips in a 24-well plate for 24 h.[40,41] The cells were incubated with either vehicle or different concentrations of complex **9** for an additional 24 h. Then, cells were collected by cytospinning at 2400 rpm for 10 min at 25 °C. The cells were washed twice with PBS and stained with FITC-labeled Annexin V (apoptosis kit, Santa Cruz Biotechnology, Santa Cruz, CA) as per the manufacturer's protocol. The coverslips were observed in a square cover glass dish with an Eclipse TE 2000U microscope (Nikon, Tokyo, Japan) at 40× magnification. The images were analyzed using *Image-Pro Plus* software (Media Cybernetics, Silver Spring, MD).

DNA Fragmentation Assay To Determine the Apoptosis. MCF-7 cells were seeded in a 25 mL culture flask. After the cell density reached $\sim 1 \times 10^6$ cells/mL, the cells were incubated without or with complex **9** ($2IC_{50}$ and $4IC_{50}$) for 48 h. After treatment, the cells were trypsinized and collected by centrifugation. The pellet was washed with PBS, dissolved in lysis buffer (50 mM pH 8.0/10 mM ethylenediaminetetraacetic acid/0.5% sL-sarcosine/0.5 mg/mL of proteinase K), and incubated at 50 °C for 1 h in a heating block.[42] After heat treatment, 5 μL of RNase (1 mg/mL) was added to the mixture and incubated at 50 °C for 1 h. Finally, the mixture was incubated at 65 °C for 2 min. Samples were allowed to cool to 25 °C and electrophoresed on 1.8% agarose DNA gel. Then DNA bands were analyzed using UV gel doc.

DNA Integrity and Cell Viability of MCF-7 and HeLa Cells Using Hoechst. MCF-7 and HeLa cells were seeded on glass coverslips in a 24-well plate at a density of 0.5×10^5 cells/mL. After 24 h of seeding, the cells were incubated without and with different concentrations of complex **9** for 24 h. The cells were collected by cytospinning at 2400 rpm for 10 min at 25 °C, fixed with formaldehyde, and permeabilized with ice-cold methanol for 20 min. Subsequently, the coverslips were rinsed with PBS and incubated with Hoechst 33258 (1 μg/mL) for 10 min in the dark at 25 °C. Hoechst 33258 was removed by washing the coverslips twice with PBS, and the samples were observed under an Eclipse TE 2000U microscope (Nikon, Tokyo, Japan) at 40× magnification. The images were analyzed using *Image-Pro Plus* software (Media Cybernetics, Silver Spring, MD).

Transfection of MCF-7 Cells with GFP-p53. MCF-7 cells were transfected with recombinant plasmid having GFP-p53 using the protocol described previously.[39,40]

Immunofluorescence Microscopy. MCF-7 cells were grown on glass coverslips at a density of 0.5×10^5 cells/mL in 24-well tissue culture plates for 24 h. Then, cells were incubated without or with different concentrations of complex **9** for another 24 h. Immunofluorescence analysis was performed as described earlier.[40,41] Cells were fixed with 3.7% formaldehyde for 30 min at 37 °C and washed twice with PBS. To block nonspecific binding, the cells were incubated with 2% bovine serum albumin (BSA)/PBS at 37 °C for 30 min. Subsequently, cells were incubated with mouse monoclonal p53 antibody (1:300 dilution in 2% BSA), mouse monoclonal anti-p21 antibody (1:300 dilution in 2% BSA), or mouse monoclonal anticyclin B1 antibody (1:300 dilution in 2% BSA) for 2 h at room temperature. The cells were washed with 2% BSA/PBS and incubated with Alexa 568-labeled antimouse IgG antibody (1:400 dilutions in 2% BSA) at room temperature for 1 h. The coverslips were rinsed with PBS and incubated with Hoechst 33258 (1 μg/mL) for 10 min in the dark at room temperature. The coverslips were then washed twice with PBS and mounted in 80% glycerol in PBS containing 8 mg/mL of 1,4-diazabicyclo[2.2.2]octane. The coverslips were then observed using an Eclipse TE 2000U microscope (Nikon, Tokyo, Japan) at 40× magnification. The images were analyzed using *Image-Pro Plus* software (Media Cybernetics, Silver Spring, MD). MCF-7 cells having GFP-p53 were also observed under an Eclipse TE 2000U microscope (Nikon, Tokyo, Japan) at 40× magnification.

X-ray Crystallography. A crystal of each of the compounds **9** and **10** suitable for single-crystal X-ray analysis was mounted in a Cryoloop with a drop of paratone oil and placed in the cold nitrogen stream of the Kryoflex attachment of the Bruker APEX CCD diffractometer. Full spheres of data were collected using 606 scans in ω (0.3° per scan) at $\phi = 0$, 120, and 240° (**9**) or a combination of three sets of 400 scans in ω (0.5° per scan) at $\varphi = 0$, 90, and 180° plus two sets of 800 scans in φ (0.45° per scan) at $\omega = -30$ and 210° (**10**) under the control of the *APEX2* software package.[43] The raw data were reduced to F^2 values using the *SAINT* software,[44] and global refinements of the unit cell parameters were performed using 9869 and 9901 reflections for **9** and **10**, respectively, which were chosen from the full data sets. For **10**, an analysis of 372 reflections chosen from diverse regions of reciprocal space (CELL_NOW)[45] indicated that the crystal belonged to the triclinic system and was twinned by a 180° rotation about c^*. For this compound, the reduction of the raw data to F^2 values was accomplished with the two-component version of *SAINT*, with the unit cell parameters for twin component 2 constrained to be the same as those for component 1. Multiple measurements of equivalent reflections provided the basis for empirical absorption corrections as well as corrections for any crystal deterioration during the data collection (*SADABS*[46a] for **9** and *TWINABS*[46b] for **10**). The structures were solved by Patterson methods and refined by full-matrix least-squares procedures using the *SHELXTL* program package.[47,48] Hydrogen atoms were placed in calculated positions and included as riding

(37) Papazisis, K. T.; Geromichalos, G. D.; Dimitriadis, K. A.; Kortsaris, A. H. *J. Immunol. Methods* **1997**, *208*, 151–158.
(38) Mohan, R.; Banerjee, M.; Ray, A.; Manna, T.; Wilson, L.; Owa, T.; Bhattacharyya, B.; Panda, D. *Biochemistry* **2006**, *45*, 5440–5449.
(39) Mohan, R.; Panda, D. *Cancer Res.* **2008**, *68*, 6181–6189.
(40) Rathinasamy, K.; Panda, D. *Biochem. Pharmacol.* **2008**, *76*, 1669–1680.
(41) Rathinasamy, K.; Panda, D. *FEBS J.* **2006**, *273*, 4114–4128.
(42) Zhu, N.; Wang, Z. *Anal. Biochem.* **1997**, *246*, 155–158.
(43) *APEX2*, version 2.1-4; Bruker-AXS: Madison, WI, 2007.
(44) *SAINT+*, version 7.34A; Bruker-AXS: Madison, WI, 2006.
(45) Sheldrick, G. M. *CELL_NOW*; University of Göttingen: Göttingen, Germany, 2005.
(46) (a) Sheldrick, G, M. *SADABS*, version 2007/2; University of Göttingen: Göttingen, Germany, 2007. (b) Sheldrick, G. M. *TWINABS*, version 2007/2; University of Göttingen: Göttingen, Germany, 2007.

contributions, with isotropic displacement parameters tied to those of the attached non-hydrogen atoms. Pertinent crystallographic data and other experimental details are summarized in Table 1.

Acknowledgment. We are thankful to the Department of Science and Technology, New Delhi, India, for financial support. J.T.M. thanks the Louisiana Board of Regents for the purchase of the CCD diffractometer and the Chemistry Department of Tulane University for support of the X-ray laboratory. D.P. is thankful for a Swarnajayanti Fellowship.

(47) Sheldrick, G. M. *SHELXS-97 and SHELXL-97*; University of Göttingen: Göttingen, Germany, 1997.
(48) Wyllie, A. H. *Nature* **1980**, *284*, 555–556.

Note Added after ASAP Publication. This paper was published on the Web on September 2, 2010. Changes were made in the paragraphs describing the syntheses of compounds **6**−**10** and the corrected version was reposted on September 7, 2010.

Supporting Information Available: X-ray crystallographic files in CIF format for the structure determinations of **9** and **10**. This material is available free of charge via the Internet at http://pubs.acs.org.